Journal of Computational Chemistry

WILEY

Journal of COMPUTATIONAL CHEMISTRY

RESEARCH ARTICLE OPEN ACCESS

Assessment of DFT Functionals for Predicting the Magnetic Exchange Coupling Constants of Nonalternant Hydrocarbon Diradicals: The Role of Hartree–Fock Exchange

Suranjan Shil

Manipal Centre for Natural Sciences, Manipal Academy of Higher Education, Manipal, Karnataka, India

Correspondence: Suranjan Shil (suranjan.shil@manipal.edu)

Received: 15 July 2024 | **Revised:** 1 October 2024 | **Accepted:** 3 November 2024

Funding: This work was supported by Science and Engineering Research Board grant no. SRG/2022/000822.

Keywords: DFT functionals | hydrocarbon | magnetic exchange coupling constant | non-alternant

ABSTRACT

The magnetic nature of nonalternant hydrocarbon (Azulene) bridged nitronyl nitroxide ($AzNN_2$) and imino-nitroxide ($AzIN_2$) diradicals are investigated with 38 different DFT functionals to find out a correct functional to predict the magnetic nature of these diradicals. The effect of Hartree–Fock exchange (HFX) in the hybrid functionals are investigated for the prediction of magnetic nature of the nonalternant hydrocarbon bridged diradicals. The utility of Borden and Davidson's proposal of disjoint and nondisjoint SOMOs for the prediction of magnetic nature of alternant hydrocarbon bridged diradicals is assessed for the non-alternant hydrocarbon based diradicals. The more affordable meta-GGA functionals was found to be outperforming the costlier hybrid and double-hybrid functionals in predicting the magnetic properties of nonalternant hydrocarbon-bridged diradicals. HFX significantly influences a functional's ability to predict a diradical's magnetic nature. Interestingly, Borden and Davidson's concept of disjoint and nondisjoint SOMOs, which is used to predict the magnetic behavior of alternant hydrocarbon diradicals, is reversed for nonalternant hydrocarbon-bridged diradicals. The difference in the magnetic nature of the two diradicals come from the canonical molecular orbitals of the diradicals, one has set of disjoint SOMOs and other has nondisjoint SOMOs.

1 | Introduction

Magnetic exchange coupling between organic radicals through alternant π-systems has been extensively studied experimentally [1–4] and theoretically [5–18]. The existing theoretical model is adequate to explain the magnetic nature of the diradical systems of alternant hydrocarbons. For the theoretical prediction of the magnetic nature of molecules, density functional theory (DFT) is widely applied. The DFT results of magnetic interaction of diradical systems with alternating hydrocarbons are compared with the experimental results, and the results of ab initio methods such as CASSCF, CASPT2, and NEVPT2. Nonalternant hydrocarbons show strange physical and chemical properties [19–21], such as the breakdown of the interference rule [19]. Azulene (Az) is an aromatic hydrocarbon with a nonalternating double bond in its ground state, antiaromatic in the first excited state and again aromatic in the second excited state [22]. It has a five-membered, electron-rich ring and a seven-membered, electron-deprived ring, which enables Az to provide intrinsic redox activity [23].

On the other hand, diradical systems of nonalternant hydrocarbons are less explored experimentally and theoretically [3]. Hewitt et al. [2] synthesized nonalternant hydrocarbon-based diradicals. The inference of their work is that Az-bridged diradicals do not follow the rule of magnetic interaction like alternant

hydrocarbon bridged diradicals [3, 24–26]. Haraguchi and coworkers [3] synthesized nonalternant hydrocarbon (azulene)-based bis-nitronyl nitroxide and bis-imino nitroxide diradicals. Surprisingly, they found that bis-nitronyl nitroxide diradicals show intramolecular ferromagnetic interactions, whereas bis-imino nitroxide diradicals show intramolecular antiferromagnetic interactions. This behavior is quite surprising because both diradicals have the same number of atoms between radical centers. In their study, they found that the hybrid density functionals could not predict the experimental results of magnetic interaction for bis-imino nitroxide diradicals but correctly predicted the magnetic nature of bis-nitronyl nitroxide diradicals, and used the experimental geometry to calculate the magnetic exchange coupling constant.

The presence of HF exchange (HFX) in DFT functionals plays a crucial role to calculate molecular properties. Calculation of magnetic exchange coupling constant with DFT depends on the percentage of HFX in the functional. It has been shown that approximately 15% HFX hybrid functionals give most accurate results [27]. By keeping this point in mind, we have calculated the magnetic exchange coupling constant with hybrid DFT functionals with varying HFX in the functionals. Cho et al. [28] studied the effect of HFX on the calculation of magnetic exchange coupling constant and they found that the low value of HFX is better to produce experimental findings.

In this work we chose Az-bridged nitronyl nitroxide (NN) and imino nitroxide (IN) diradicals (Figure 1), which were experimentally synthesized, and the magnetic exchange coupling constant was measured experimentally [3]. The objective of this work is two fold: (i) finding an appropriate density functionals that can correctly predict the magnetic nature of nonalternant hydrocarbon bridged diradicals and (ii) determine why Az-bridged NN and IN diradicals show opposite magnetic natures in contrast to aromatic alternant hydrocarbon bridged diradicals.

2 | Theoretical and Computational Details

We optimized all the molecular structures in their high spin state using all 38 functionals taken in this work in combination with the def2-TZVP basis set. We use the Yamaguchi [29] formula for the evaluation of the magnetic exchange coupling constant J for all the systems, depicted as:

$$J = \frac{E_{BS} - E_{HS}}{\left\langle \hat{S}^2 \right\rangle_{HS} - \left\langle \hat{S}^2 \right\rangle_{BS}} \quad (1)$$

where E_{BS} and E_{HS} and $\left\langle \hat{S}^2 \right\rangle_{BS}$ and $\left\langle \hat{S}^2 \right\rangle_{HS}$ are the energy and average spin square values of the BS states and their corresponding high-spin states, respectively. Positive and negative values of J correspond to ferromagnetic and antiferromagnetic coupling, respectively. To confirm the BS solutions of the wave functions we have checked the spin square values of the triplet and BS state with all the functionals given in the Supporting Information. To test the consistency of the J values we have calculated it with spin unprojected formulae given in the Supporting Information.

All calculations were performed using spin-unrestricted KS-DFT employing the ORCA 5.0.1 program package [30]. The visualization of molecular structure, molecular orbitals and so forth, has been carried out using Avogadro software [31].

3 | Results and Discussion

DFT functionals from across the Jacob's ladder has been chosen to test the predictive power of each functional for the magnetic exchange coupling constant of nonalternant hydrocarbon (azulene) bridged diradicals. At the same time, we focused on the hybrid DFT functionals as these functionals are known to be good for magnetic property prediction. The % of HFX in different hybrid functionals are tested and tried to understand the effect on the magnetic exchange coupling constant of the diradicals under study. Another debatable argument for testing performance of different methodology whether we should calculate a desired property on same geometry or optimize the geometry in each method. In our earlier works [32, 33], we optimized all the geometries using various functionals, arguing that for a new molecule without experimental geometry, it is essential to first determine the geometry before predicting its properties. If we calculate on the same geometry and perform property calculation, then there is no point

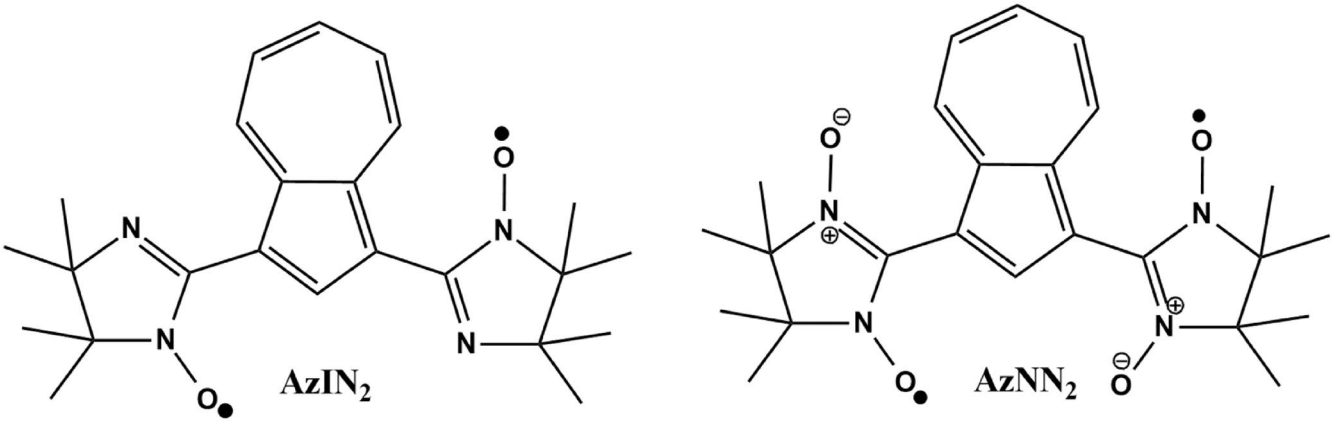

FIGURE 1 | Azulene bridged imino nitroxide ($AzIN_2$) and nitronyl nitroxide ($AzNN_2$) diradicals.

of testing the validity of the methods. In that case we obtain the geometries from different methods and then calculate the properties. Here, in this study we follow both the methodology (i) optimize the geometry in each functionals and then calculate the magnetic exchange coupling constant with the same functionals and (ii) calculation of magnetic exchange coupling constant on same geometry.

3.1 | Efficiency of Local and Gradient Corrected Functionals

In the local spin density (LSD) approximation, the exchange correlation functional can be defined as.

$$E_{XC}^{\mathrm{LSD}}\left[n_{\uparrow},n_{\downarrow}\right]=\int d^{3}r\, n\epsilon_{XC}^{\mathrm{unif}}\left(n_{\uparrow},n_{\downarrow}\right) \tag{2}$$

where $n_{(\uparrow)}(r)$ and $n_{(\downarrow)}(r)$ are the electron spin densities and $\epsilon_{XC}^{\mathrm{unif}}$ is the exchange correlation energy per particle of a uniform electron gas.

When $n=n_{\uparrow}+n_{\downarrow}$, is the generalized gradient approximation (GGA) exchange correlation functional can be expressed as [34, 35].

$$E_{XC}^{\mathrm{GGA}}\left[n_{\uparrow},n_{\downarrow}\right]=\int d^{3}r f\left(n_{\uparrow},n_{\downarrow},\Delta n_{\uparrow},\nabla n_{\downarrow}\right) \tag{3}$$

GGA has several advantages over LSD in terms of total energy calculation, atomization energies, energy barriers and structural energy differences [34, 36–41] The GGA functionals account for the realistic fact that a molecule's electron density is not spatially uniform.

In Table 1, we present the computed magnetic exchange coupling constants for $AzIN_2$ and $AzNN_2$ using 11 different local and gradient-corrected functionals. The data in Table 1 reveals that all the functionals consistently yield accurate results for antiferromagnetically coupled $AzIN_2$ diradicals. However, for ferromagnetically coupled $AzNN_2$ diradicals, the functionals provide divergent predictions. These findings suggest that local functionals show promise in predicting the behavior of antiferromagnetically coupled diradicals that are linked through Az, a nonalternant hydrocarbon. LSD and GGA functionals has no admixture of HFX part in them, which is required to capture the exchange interaction in ferromagnetic complexes. The lack of HFX in the LSD and GGA is one of the reasons not to correctly predict the ferromagnetic interaction. Calculation of magnetic exchange coupling constant on optimized geometry of each functional and on the B3LYP optimized geometry gives similar qualitative results (Table 1).

3.2 | Efficiency of Meta GGA Functionals

Meta GGA functionals take into account the local kinetic energy density, which enables them to be more accurate than GGAs. The general form of the meta-GGA functional can be written as.

$$E_{XC}^{\mathrm{mGGA}}\left[n_{\uparrow},n_{\downarrow}\right]=\int d^{3}r f\left(n_{\uparrow},n_{\downarrow},\Delta n_{\uparrow},\nabla n_{\downarrow},\tau_{\uparrow},\tau_{\downarrow}\right) \tag{4}$$

where,

$$\tau_{\sigma}(r)=\sum_{i}^{\mathrm{occup}}\frac{1}{2}\left|\nabla\psi_{i\sigma}(r)\right|^{2} \tag{5}$$

is the kinetic energy density for the occupied Kohn–Sham orbitals $\psi_{i\sigma}(r)$, which are nonlocal functionals of the density $n_{\sigma}(r)$.

We can see from Table 1 that the revTPSS functional predicts the correct sign of the magnetic exchange coupling constant for antiferromagnetic diradicals on B3LYP geometry as well as on optimized structure. Whereas TPSS and M06L predicts the correct sign of magnetic interaction of ferromagnetic and antiferromagnetic diradicals when optimized in each functionals. The unexpected correctness of M06L functional does not come from a well-suited exchange or correlation part of the functional. Instead, it is believed to arise from a fortuitous cancellation of errors [42]. Meta-GGA functional contains nonlocal part in the form of kinetic energy density which makes them superior to the GGA. This added correction over GGA enables meta-GGA functional to predict the sign of ferromagnetic interaction in the diradicals. However, the single point calculation on B3LYP geometry gives inconsistent results for ferromagnetic diradicals except M06L functional.

3.3 | Efficiency of Hybrid Functionals

Hybrid functionals are the most successful for the calculation of the magnetic exchange coupling constant of the organic diradical, especially the B3LYP functional. The general form of a hybrid DFT functional can be expressed as [41].

$$E_{XC}=E_{XC}^{\mathrm{LSDA}}+a_{0}\left(E_{X}^{\mathrm{exact}}-E_{X}^{\mathrm{LSDA}}\right)+a_{X}\Delta E_{X}^{B88}+a_{C}\Delta E_{C}^{\mathrm{PW91}}, \tag{6}$$

where $a_0, a_X, and\ a_C$ are semiempirical coefficients to be determined by an appropriate fit to experimental data, E_X^{exact} is the exact exchange energy, ΔE_X^{B88} is Becke's 1988 gradient correction (to the LSDA) for exchange [43], and $\Delta E_C^{\mathrm{PW91}}$ is the 1991 gradient correction for the correlation of Perdew and Wang [36, 44].

In Table 1, the magnetic exchange coupling constants of the Az-coupled diradicals with all the functionals are listed. All the hybrid functionals predict qualitatively correct results for ferromagnetically coupled diradicals, whereas they give opposite results for antiferromagnetically coupled diradicals. This is because hybrid functionals are biased to the high spin state. Among the four hybrid functionals, the BHANDHLYP functional abruptly overestimates the coupling constant for the ferromagnetically coupled diradical. The hybrid functionals contains HFX part in them from 10% to 100% which makes them enable to predict ferromagnetic interaction correctly however, disabled them to predict the correct antiferromagnetic interactions. Fine tuning of the HFX in them could have enabled them to predict the ferro and antiferromagnetism both accurately. All the hybrid functionals gives inconsistent results for antiferromagnetic diradical with both of the methods single point and optimization of geometry.

TABLE 1 | The magnetic exchange coupling constant of the diradicals with all the functional and def2-TZVP basis sets.

	Single point on B3LYP optimized geometry		Optimized in each functional	
	$AzIN_2$	$AzNN_2$	$AzIN_2$	$AzNN_2$
Systems		J (cm^{-1})		
Experiment	−3.06 (−4.4 K)	6.95 (10 K)	−3.06 (−4.4 K)	6.95 (10 K)
Local and gradient corrected functionals				
HFS	−1.63	−3.52	−2.28	−3.02
LSD	−1.15	−2.87	−0.82	−3.84
VWN5	−0.90	−3.41	−0.84	−3.84
VWN3	−0.75	−3.06	−0.57	−3.80
PWLDA	−1.15	−2.86	−0.78	−3.87
BP86	−0.99	−2.11	−1.16	−2.29
PBE	−1.03	−2.33	−1.04	−2.39
RPBE	−1.04	−1.69	−0.58	−1.89
PW91	−1.11	−2.37	−1.07	−2.45
mPWPW	−1.01	−2.10	−0.97	−2.24
Meta-GGA functionals				
TPSS	−0.55	−0.28	**−1.52**	**0.01**
M06L	0.24	2.53	**−0.59**	**0.24**
revTPSS	−0.58	−0.52	−1.46	−0.69
Hybrid functionals				
B3LYP	3.60	12.42	3.18	12.17
PBE0	8.44	32.52	7.45	32.88
PW6B95	4.01	15.51	3.38	9.40
BHANDHLYP	66.95	217.65	52.99	203.80
TPSSh	2.55	9.76	1.96	10.50
TPSS0	15.34	55.68	12.97	55.96
M06	4.39	17.98	3.26	12.97
M062X	3.89	23.53	3.13	17.55
B97M-V	0.73	3.12	0.94	1.19
B97M-D3BJ	1.01	3.63	1.18	1.95
Range-separated hybrid functionals				
ωB97	46.57	23.6626	37.77	225.36
ωB97X	28.53	144.59	22.67	125.36
ωB97X-D3	19.30	98.81	15.79	74.99
ωB97X-D3BJ	21.75	117.01	18.43	97.87
ωB97X-V	9.46	113.41	17.78	93.59
ωB97M-V	9.46	58.35	59.67	66.04
ωB97M-D3BJ	9.82	60.36	58.77	67.26
CAM-B3LYP	18.68	84.09	15.35	75.61

(Continues)

TABLE 1 | (Continued)

	Single point on B3LYP optimized geometry		Optimized in each functional	
	$AzIN_2$	$AzNN_2$	$AzIN_2$	$AzNN_2$
Systems		J (cm^{-1})		
LC-BLYP	16.80	93.15	12.93	93.16
Perturbatively corrected double-hybrid functionals				
B2PLYP	136.35	351.14	99.07	252.75
mPW2PLYP	156.08	384.50	108.67	284.92
B2GP-PLYP	98.15	753.22	250.22	536.58
Range-separated double-hybrid functionals				
ωB2PLYP	78.85	790.31	257.40	625.83
ωB2GP-PLYP	735.67	1100.01	446.88	870.61

Note: The bold values represent the functionals which give correct signs of magnetic exchange coupling constant for both the complexes.

3.4 | Efficiency of Hybrid Meta-GGA Functionals

We can formulate a global hybrid version of the novel MGGA functional by blending TPSS with exact exchange, which can be expressed as follows:

$$E_{XC}^{\text{hybrid-mGGA}} = aE_X^{\text{exact}} + (1-a)E_X^{\text{mGGA}} + E_C^{\text{mGGA}} \tag{7}$$

where a is an empirical parameter fit to experimental data for atomization energies and E_X^{mGGA} is the energy density meta-generalized approximation [45] for exchange, is constructed using Becke's inhomogeneity parameter [46].

All the hybrid meta GGA functionals give inaccurate predictions of antiferromagnetically coupled diradicals. However, these functionals predict the exact sign of the magnetic exchange coupling constant of the ferromagnetic diradical. Therefore, it can be said that the hybrid meta GGA functionals are good for ferromagnetic diradicals and cannot be used for antiferromagnetic diradicals based on nonalternant hydrocarbon. The hybrid meta GGA functionals are further corrected over hybrid functional and eventually overestimated the ferromagnetic interaction in the diradicals. All the hybrid functionals gives inconsistent results for antiferromagnetic diradical with both of the methods single point and optimization of geometry.

3.5 | Efficiency of Range-Separated Hybrid Functionals

The range-separated hybrid functionals are designed on the basis of the smooth partition into short range (SR) and long range (LR) parts of the Coulomb operator, $1/r$, as:

$$\frac{1}{r} = \left\{\frac{\text{erfc}(\omega r)}{r}\right\}_{\text{SR}} + \left\{\frac{\text{erf}(\omega r)}{r}\right\}_{\text{LR}} \tag{8}$$

by the inclusion of short-range $erfc(\omega r)$ and long-range $erf(\omega r)$ functions, the two smooth weighing functions, where ω is the parameter describing part of the separation, and r is the interelectronic distance. These smooth weighting functions are the Gauss error functions and complementary Gauss error functions. These functions have the properties that $\text{erf}(0)=0$, $\text{erf}(\infty)=1$, $\text{erfc}(0)=1$ and $\text{erfc}(\infty)=0$. Based on this partitioning scheme we can divide the exchange energy into two parts:

$$E_X = E_X^S(\omega) + E_X^L(\omega) \tag{9}$$

Using this partitioning scheme, many different range-separated functionals have been designed [47–62].

The range-separated hybrid functionals give the wrong sign for the magnetic exchange coupling constant of antiferromagnetically coupled diradicals (Table 1). However, they predict the correct sign of the magnetic exchange coupling constant of ferromagnetic diradicals, although they overestimate the value of the coupling constant. All the hybrid functionals gives inconsistent results for antiferromagnetic diradical with both of the methods single point and optimization of geometry.

3.6 | Efficiency of Perturbatively Corrected Double-Hybrid Functionals

The amalgamation of KS-DFT and perturbation theory (PT) is founded on the subsequent expression for the exchange-correlation energy, denoted as E_{XC}, and is explicitly provided as follows: [63].

$$E_{XC} = (1-a_X)E_{XC}^{\text{GGA}} + a_X E_X^{\text{HF}} + bE_C^{\text{GGA}} + cE_C^{\text{PT2}} \tag{10}$$

where (in the spin-orbital form)

$$E_C^{\text{PT2}} = \frac{1}{4}\sum_{ia}\sum_{jb}\frac{\left[(ia|jb)-(ib|ja)\right]^2}{\epsilon_i+\epsilon_j-\epsilon_a-\epsilon_b} \tag{11}$$

The expression presented is a conventional second-order Møller–Plesset-type equation for the correlation energy.

However, it is assessed using the Kohn–Sham orbitals with their corresponding eigenvalues. The indices ia and *jb* signify single occupied-virtual replacements, and the terms enclosed in brackets represent standard two-electron integrals over the Kohn–Sham orbitals.

In Equation (10), a_X signifies the HFX mixing parameter, while *b* and *c* correspond to the GGA and perturbative correlation contributions, respectively.

The expensive perturbatively corrected double-hybrid functionals predict the opposite sign of the magnetic exchange coupling constant of the antiferromagnetic diradical. However, it predicts the correct sign of magnetic coupling for ferromagnetic diradicals, although there is a very high overestimation of the coupling constant. All the hybrid functionals gives inconsistent results for antiferromagnetic diradical with both of the methods single point and optimization of geometry.

3.7 | Efficiency of Range-Separated Double-Hybrid Functionals

The range-separated double hybrid functionals ωB2PLYP and ωB2GPPLYP can be written as [64].

$$E_{XC}^{\omega\text{B2PLYP}} = 0.47E_X^{\omega B88}(\omega) + 0.53E_X^{\text{SR-HF}} + E_X^{\text{LR-HF}} + 0.73E_C^{\text{LYP}} + 0.27E_C^{\text{nonlocal}} \tag{12}$$

$$E_{XC}^{\omega\text{B2GPPLYP}} = 0.35E_X^{\omega B88}(\omega) + 0.65E_X^{\text{SR-HF}} + E_X^{\text{LR-HF}} + 0.64E_C^{\text{LYP}} + 0.36E_C^{\text{nonlocal}} \tag{13}$$

In both the methods, the exchange components are divided into two parts: SR (short range) and LR (long range). The SR exchange part consists of scaled and SR-adjusted Becke-88 exchange [62] (ωB88) and Fock exchange (ExSR-HF), while the LR exchange part comprises unscaled Fock exchange (ExLR-HF).

Regarding the correlation components, they are identical to those found in B2PLYP and B2GPPLYP, which involve a combination of scaled Lee, Yang, and Parr [65] (LYP) correlation and scaled nonlocal correlation. Specifically, for ground states, this nonlocal correlation is derived from MP2, and for excited states, it is obtained from CIS(D).

The computationally expensive range-separated double-hybrid functionals predict the exact sign of the magnetic exchange coupling constant of ferromagnetic diradicals with very high overestimation of the coupling constant values. However, it fails to predict the correct sign of the magnetic coupling of antiferromagnetic diradicals.

The above analysis of all types of functionals reveals that the LSD and GGA functional hold good for antiferromagnetic coupling, meta-GGA functionals (TPSS and M06L) predicts exact sign of ferromagnetic and antiferromagnetic coupling. The hybrid and other sophisticated functionals are overestimated the ferromagnetic interaction and wrongly predict the antiferromagnetic coupling. The qualitative reason for such behavior is the presence and absence of HFX in the functionals. All the hybrid functionals gives inconsistent results for antiferromagnetic diradical with both of the methods single point and optimization of geometry.

Figure 2a–g displays a visual look of the performance of all the functionals studied here in this work.

3.8 | Geometrical Parameters of the Diradicals With Different Functionals

The geometry of molecules is very important for the magnetic interaction in organic diradicals where the magnetic interaction occurs via itinerant exchange [10, 66]. The planarity of radical and the coupler plays an important role in the magnetic interaction in diradical molecules. The geometrical parameters of the diradicals studied here are given in Table 2. We can observe from the Table 2 that the distance between radical and the couplers are same (1.45 Å) for both the diradicals in the crystal structure (experiment), however, the dihedral angle between the radical and coupler is high (40°) for the NN diradical which is ferromagnetic in nature. On the other hand, IN diradical the dihedral angle between the radical and coupler is low (4.3° and 8.8°) and the diradical is antiferromagnetic in nature. Now if we see the calculated values of radical-coupler distance it varies from 1.43 to 1.46 Å which is close to the experimental values as compared to the range of the dihedral angle which is huge (for IN diradical it is from 7° to 24°; and for NN diradical it is from 23° to 37°). Careful inspection of the Table 2 turns out that local functionals give lower dihedral angle and range separated hybrid functionals gives higher values of dihedral angle and of course this is not uniform. This could be a reason why the local functionals give correct results for IN diradicals and the hybrid and expensive functionals give correct sign of magnetic coupling of NN diradical as they reach the near experimental geometry with the respective functionals.

3.9 | Effect of the HFX Parameter in Hybrid Functionals to Predict the Magnetic Exchange Coupling Constant

To investigate the effect of HFX on the calculation of the magnetic exchange coupling constant, we choose three hybrid functionals, namely, B3LYP (HFX 20%), M06 (HFX 27%), and M06-2X (HFX 54%). The % of HFX versus magnetic exchange coupling constant plots are given in Figure 3. From Figure 3, we can observe that in every functional, there is a crossing point where the coupling constant changes its sign for both the diradical ferromagnetic and antiferromagnetic molecules. Most importantly, every functional gives a correct prediction of the magnetic exchange coupling sign for both diradicals at a certain value of HFX. For B3LYP 11%, HFX predicts the correct sign of the magnetic exchange coupling constant, and for M06 and M06-2X, these values are 20% and 42%, respectively. Below 11% HFX, the B3LYP functional predicts the correct sign of antiferromagnetic diradicals, whereas for ferromagnetic diradicals, it predicts the correct sign of magnetic exchange above 11% HFX in the functional. For the M06 functional, the optimal value of HFX is ≤ 20% for antiferromagnetic diradicals and ≥ 20% for ferromagnetic diradicals. For the M06-2X functional, the optimal value of HFX is ≤ 42% for antiferromagnetic diradicals and ≥ 42% for ferromagnetic diradicals. These results signify that

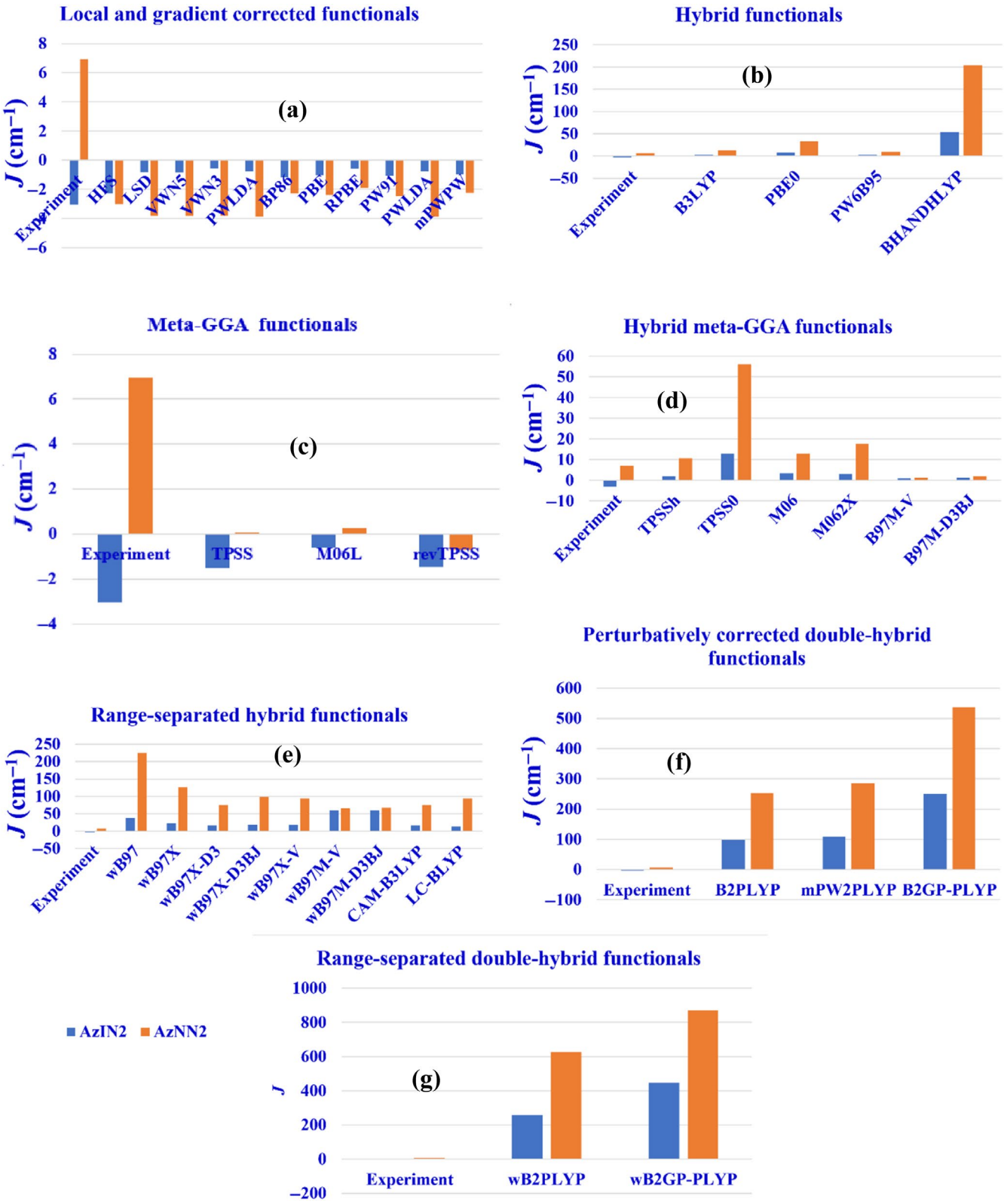

FIGURE 2 | The visual look of the performance of the functional when optimized in each functional.

the % of HFX in a functional plays a major role in the prediction of the magnetic exchange coupling constant. The so-called universal functional B3LYP failed to predict the correct nature of magnetic exchange coupling for the Az-coupled diradical. The expensive DFT functional, such as the double hybrid and range-separated double hybrid functional, overestimate the magnetic exchange coupling constant for ferromagnetic diradicals, and they are over biased towards high spin states.

TABLE 2 | Structural parameters of the diradicals with different functionals.

	$AzIN_2$				$AzNN_2$			
	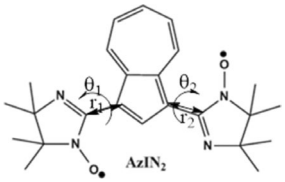				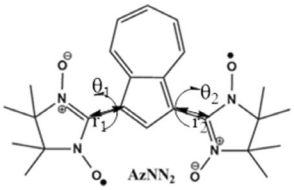			
Systems	r_1 (Å)	r_2 (Å)	θ_1 (°)	θ_2 (°)	r_1 (Å)	r_2 (Å)	θ_1 (°)	θ_2 (°)
Experiment [3]	1.45	1.45	4.30	8.80	1.45	1.45	40.38	40.38
HFS	1.45	1.45	8.66	8.66	1.45	1.45	26.12	27.88
LSD	1.43	1.43	7.30	7.30	1.43	1.43	24.85	23.79
VWN5	1.43	1.43	7.29	7.29	1.43	1.43	24.85	23.79
VWN3	1.43	1.43	7.14	7.14	1.43	1.43	24.61	23.38
PWLDA	1.43	1.43	7.30	7.30	1.43	1.43	24.87	23.81
BP86	1.45	1.45	16.85	16.85	1.45	1.45	33.32	29.81
PBE	1.45	1.45	17.12	17.12	1.45	1.45	33.57	29.79
RPBE	1.46	1.46	20.06	20.06	1.46	1.46	35.15	37.08
PW91	1.45	1.45	16.82	16.82	1.45	1.44	29.52	33.09
mPWPW	1.45	1.45	17.40	17.41	1.45	1.45	30.51	33.96
TPSS	1.45	1.45	12.13	12.14	1.45	1.45	33.10	29.61
M06L	1.44	1.44	9.75	9.75	1.44	1.43	31.77	35.97
revTPSS	1.45	1.45	12.70	12.70	1.44	1.44	29.28	33.27
B3LYP	1.45	1.45	19.83	19.83	1.45	1.45	34.91	31.24
PBE0	1.45	1.45	19.86	19.85	1.44	1.44	34.67	29.60
PW6B95	1.44	1.44	20.74	20.74	1.44	1.44	36.23	33.24
BHANDHLYP	1.45	1.45	9.81	9.81	1.44	1.44	34.78	29.48
TPSSh	1.45	1.45	18.57	18.57	1.44	1.44	33.63	29.64
TPSS0	1.45	1.45	12.25	24.24	1.44	1.44	34.29	29.29
M06	1.45	1.45	20.70	20.70	1.44	1.44	30.25	37.83
M062X	1.45	1.45	21.63	21.81	1.44	1.44	31.0	37.10
B97M-V	1.44	1.44	20.45	20.45	1.43	1.43	30.40	34.72
B97M-D3BJ	1.44	1.44	20.40	20.40	1.43	1.43	30.40	34.57
ωB97	1.46	1.46	19.15	19.15	1.45	1.45	30.60	33.03
ωB97X	1.46	1.46	21.58	21.58	1.45	1.45	31.65	36.03
ωB97X-D3	1.45	1.45	22.0	22.0	1.45	1.44	34.01	37.42
ωB97X-D3BJ	1.46	1.46	21.89	21.88	1.45	1.45	33.45	36.91
ωB97X-V	1.46	1.46	21.79	21.79	1.45	1.45	33.11	36.70
ωB97M-V	1.45	1.45	22.08	22.08	1.45	1.44	32.83	36.60
ωB97M-D3BJ	1.45	1.45	22.20	22.20	1.45	1.45	33.14	36.96
CAM-B3LYP	1.45	1.45	20.51	20.51	1.44	1.44	34.95	30.81

(Continues)

TABLE 2 | (Continued)

	$AzIN_2$				$AzNN_2$			
	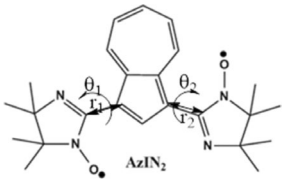				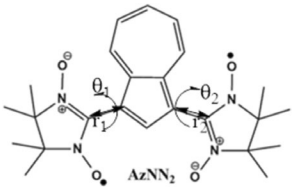			
Systems	r_1 (Å)	r_2 (Å)	θ_1 (°)	θ_2 (°)	r_1 (Å)	r_2 (Å)	θ_1 (°)	θ_2 (°)
LC-BLYP	1.45	1.45	16.17	16.17	1.44	1.44	28.67	31.01
B2PLYP	1.45	1.45	20.25	20.25	1.45	1.45	34.93	35.32
mPW2PLYP	1.45	1.45	18.88	18.88	1.45	1.45	33.78	34.45
B2GP-PLYP	1.45	1.45	18.18	18.18	1.45	1.44	32.61	34.08
ωB2PLYP	1.45	1.45	16.08	16.08	1.44	1.44	29.50	31.45
ωB2GP-PLYP	1.45	1.45	16.05	16.05	1.44	1.44	29.01	31.12

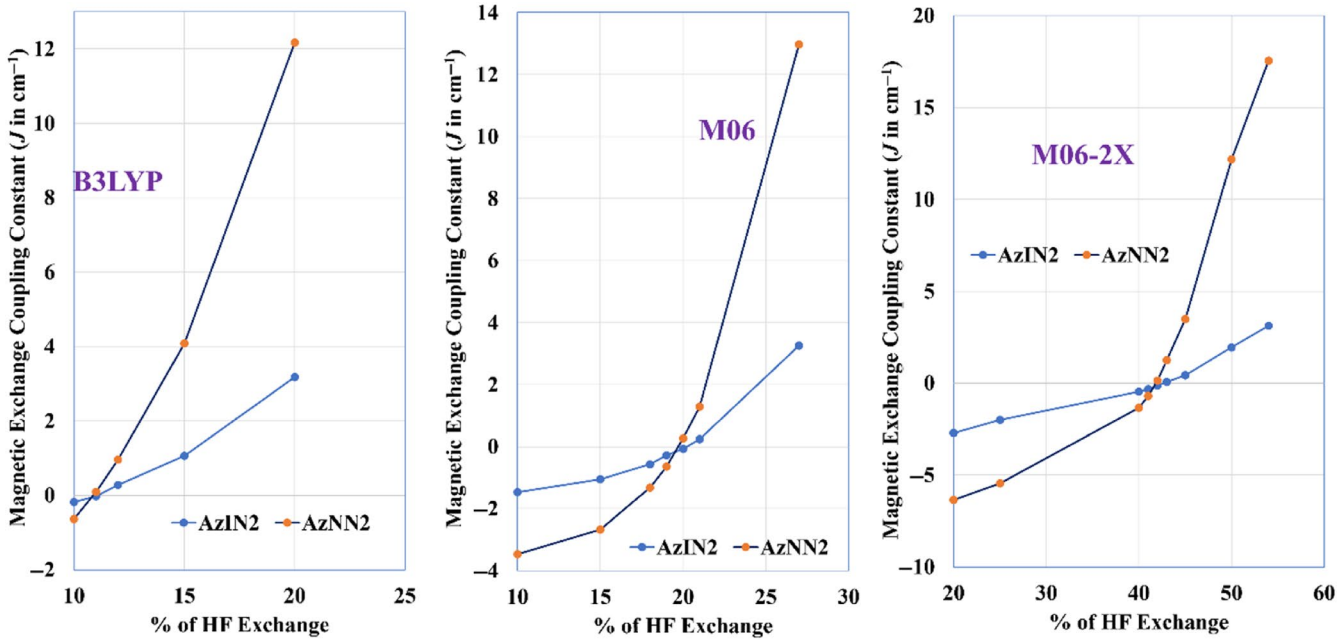

FIGURE 3 | The variation in the magnetic exchange coupling constant (J) with respect to the % of HF exchange in the functionals.

3.10 | Molecular Orbitals

Canonical molecular orbitals are often used to define the magnetic properties of diradicals. According to Borden and Davidson, nondisjoint SOMOs (which are confined to sets of atoms with no common number) favor ferromagnetic interactions, and disjoint SOMOs (atoms are common) favor antiferromagnetic interactions in case of alternant hydrocarbon diradicals. Dias [67] showed that for nonalternant hydrocarbon diradicals disjoint diradical favor nonmagnetic state whereas, nondisjoint character favored triplet state. Haraguchi et al. [3] calculated the natural orbital of the same diradicals studied here. They found that the natural orbitals of both the diradical $AzIN_2$ and $AzNN_2$ are the same and that they are disjointed. However, in our work, we found that the canonical orbital SOMOs of $AzIN_2$ are nondisjoint and that the SOMOs of $AzNN_2$ are disjoint. Nevertheless, here, for Az-coupled diradicals, this trend is the opposite of Borden and Davidson's proposal [68, 69]. Therefore, for nonalternant hydrocarbon bridged diradical disjoint-nondisjoint formula is the opposite of alternant hydrocarbon-based diradicals. In the earlier work [3] the SOMOs of both the diradicals are disjoint whereas in this work we found different SOMOs for the diradicals, the reason is that the earlier author gives the natural orbital SOMOs whereas we plotted the canonical orbitals. To rule out the alternation in SOMOs for unrestricted DFT calculation we also calculated with restricted open shell model and the result is replicated (see Supporting Information) as unrestricted calculation (Figure 4).

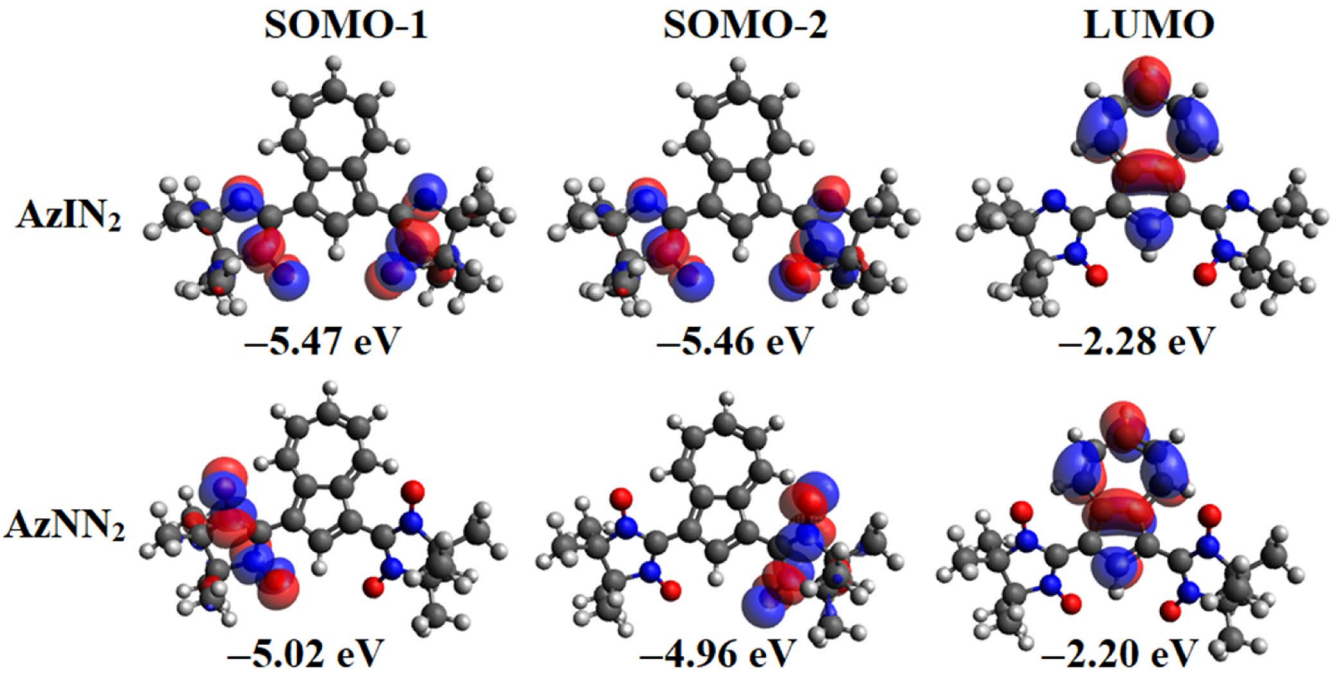

FIGURE 4 | Canonical molecular orbitals of the diradicals at the B3LYP/def2-TZVP level (iso value 0.03).

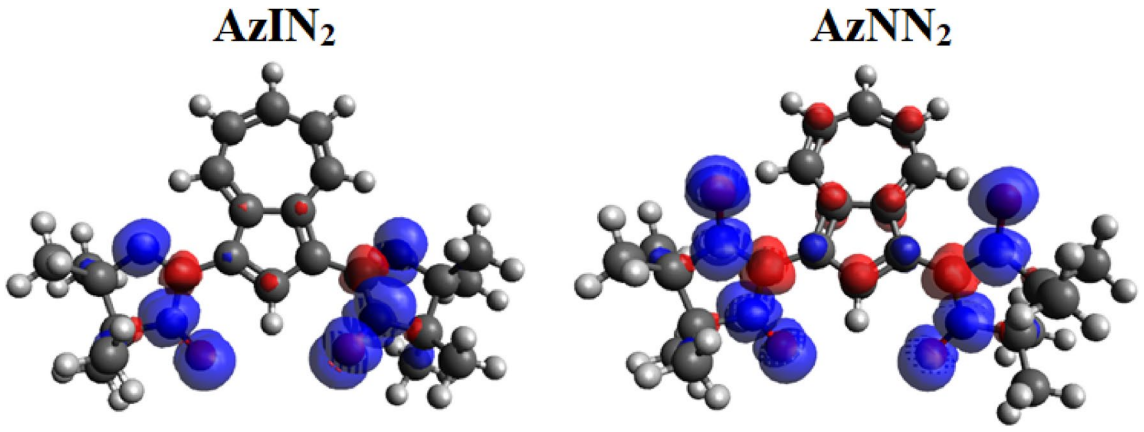

FIGURE 5 | Spin density of the diradicals in their triplet state at the B3LYP/def2-TZVP level (iso value 0.002).

3.11 | Spin Density of the Diradical

The spin density analysis gives an insight into the spin polarization of magnetic systems. The spin density plot of the diradicals is shown below in Figure 5. A close look at Figure 5 tells us that in the case of the $AzIN_2$ diradical, the spin density distribution over Az is less than that over the $AzNN_2$ diradical. This signifies that the NN diradical induce more spin polarization in the coupler compared to the IN diradical. The more spin polarization reflected in the higher absolute values of coupling constant of $AzNN_2$.

4 | Conclusions

Nonalternant hydrocarbon bridged diradicals show a different magnetic behavior compared to the alternant hydrocarbon based diradicals. We have found that the less expensive meta-GGA functionals are better due to the absence of HFX in them for the prediction of magnetic nature of nonalternant hydrocarbon bridged diradicals compared to the expensive hybrid and double hybrid functionals. This behavior in turn indicates that the over sophistication in functionals may not be good for property prediction, especially the magnetic interaction. The HFX plays a major role in a functional to predict the magnetic nature of a diradical. The value of HFX is different for different functional to predict a correct nature of magnetic interaction. The Borden and Davidson's proposal of disjoint and nondisjoint SOMOs for the prediction of magnetic nature of a diradical is opposite for nonalternant hydrocarbon bridged diradical in contrast to the alternant hydrocarbon bridged diradicals. The IN radical creates less spin polarization compared to the NN diradical in the coupler (Az).

Acknowledgments

Manipal Centre for Natural Sciences, Centre of Excellence, Manipal Academy of Higher Education (MAHE) is acknowledged for providing

the facilities and support. SERB India is acknowledged for financial support via grant no. SRG/2022/000822. This research work has also used the high computing facility (Shakti) at Manipal Centre for Natural Sciences, Manipal Academy of Higher Education.

Data Availability Statement

The data that supports the findings of this study are available in the Supporting Information of this article.

References

1. A. Rajca, S. Rajca, and J. Wongsriratanakul, "Singlet–Triplet Energy Gap in a Cyclophane-Based Organic Diradical with Parallel Exchange Coupling Pathways," *Chemical Communications* 12 (2000): 1021–1022, https://doi.org/10.1039/b001273o.

2. P. Hewitt, D. A. Shultz, and M. L. Kirk, "Rules for Magnetic Exchange in Azulene-Bridged Biradicals: Quo Vadis?," *Journal of Organic Chemistry* 86, no. 21 (2021): 15577–15587, https://doi.org/10.1021/acs.joc.1c02085.

3. M. Haraguchi, E. Tretyakov, N. Gritsan, et al., "(Azulene-1,3-Diyl)-Bis(Nitronyl Nitroxide) and (Azulene-1,3-Diyl)-Bis(Iminonitroxide) and Their Copper Complexes," *Chemistry, an Asian Journal* 12, no. 22 (2017): 2929–2941, https://doi.org/10.1002/asia.201701085.

4. A. Rajca, "Organic Diradicals and Polyradicals: From Spin Coupling to Magnetism?," *Chemical Reviews* 94, no. 4 (1994): 871–893, https://doi.org/10.1021/cr00028a002.

5. C. Trindle and S. N. Datta, "Molecular Orbital Studies on the Spin States of Nitroxide Species: Bis- and Trisnitroxymetaphenylene, 1,1-Bisnitroxyphenylethylene, and 4,6-Dimethoxy-1,3-Dialkylnitroxybenzenes," *International Journal of Quantum Chemistry* 57, no. 4 (1996): 781–799, https://doi.org/10.1002/(SICI)1097-461X(1996)57:4<781::AID-QUA26>3.0.CO;2-1.

6. M. E. Ali and S. N. Datta, "Broken-Symmetry Density Functional Theory Investigation on Bis-Nitronyl Nitroxide Diradicals: Influence of Length and Aromaticity of Couplers," *Journal of Physical Chemistry A* 110, no. 8 (2006): 2776–2784, https://doi.org/10.1021/jp057083w.

7. S. Shil and A. Misra, "Electric Field Induced Tuning of Molecular Conformation to Acquire Spintronics Property in Biphenyl Systems," *RSC Advances* 3, no. 34 (2013): 14352–14362.

8. S. Shil and A. Misra, "Photoinduced Antiferromagnetic to Ferromagnetic Crossover in Organic Systems," *Journal of Physical Chemistry A* 114, no. 4 (2010): 2022–2027.

9. P. Sarbadhikary, S. Shil, and A. Misra, "Magnetic and Transport Properties of Conjugated and Cumulated Molecules: The π-System Enlightens Part of the Story," *Physical Chemistry Chemical Physics* 20, no. 14 (2018): 9364–9375.

10. S. Shil, M. Roy, and A. Misra, "Role of the Coupler to Design Organic Magnetic Molecules: LUMO Plays an Important Role in Magnetic Exchange," *RSC Advances* 5, no. 128 (2015): 105574–105582.

11. S. Shil, S. Paul, and A. Misra, "Charge-Transfer-Induced Magnetism in Mixed-Stack Complexes," *Journal of Physical Chemistry C* 117, no. 5 (2013): 2016–2023.

12. D. Bhattacharya, S. Shil, and A. Misra, "Photoresponsive Magnetization Reversal in Green Fluorescent Protein Chromophore Based Diradicals," *Journal of Photochemistry and Photobiology A: Chemistry* 217, no. 2–3 (2011): 402–410.

13. P. Sarbadhikary, S. Shil, A. Panda, and A. Misra, "A Perspective on Designing Chiral Organic Magnetic Molecules with Unusual Behavior in Magnetic Exchange Coupling," *Journal of Organic Chemistry* 81, no. 13 (2016): 5623–5630.

14. D. Bhattacharya, S. Shil, A. Panda, and A. Misra, "A DFT Study on the Magnetostructural Property of Ferromagnetic Heteroverdazyl Diradicals with Phenylene Coupler," *Journal of Physical Chemistry A* 114, no. 43 (2010): 11833–11841.

15. K. C. Ko, D. Cho, and J. Y. Lee, "Scaling Approach for Intramolecular Magnetic Coupling Constants of Organic Diradicals," *Journal of Physical Chemistry A* 117, no. 16 (2013): 3561–3568, https://doi.org/10.1021/jp4017695.

16. K. C. Ko, D. Cho, and J. Y. Lee, "Systematic Approach To Design Organic Magnetic Molecules: Strongly Coupled Diradicals with Ethylene Coupler," *Journal of Physical Chemistry A* 116, no. 25 (2012): 6837–6844, https://doi.org/10.1021/jp211225j.

17. S. Shil, D. Bhattacharya, A. Misra, Y. P. Ortiz, and D. J. Klein, "The Effect of Hetero-Atoms on Spin Exchange Coupling Pathways (ECPs): A Computational Investigation," *Physical Chemistry Chemical Physics* 25, no. 21 (2023): 14786–14798, https://doi.org/10.1039/d3cp00394a.

18. C. Trindle, S. N. Datta, and B. Mallik, "Phenylene Coupling of Methylene Sites. The Spin States of Bis(X–methylene)-*p*-Phenylenes and Bis(Chloromethylene)-*m*-Phenylene," *Journal of the American Chemical Society* 119, no. 52 (1997): 12947–12951, https://doi.org/10.1021/ja9704139.

19. J. Xia, B. Capozzi, S. Wei, et al., "Breakdown of Interference Rules in Azulene, a Nonalternant Hydrocarbon," *Nano Letters* 14, no. 5 (2014): 2941–2945, https://doi.org/10.1021/nl5010702.

20. M. Beer and H. C. Longuet-Higgins, "Anomalous Light Emission of Azulene," *Journal of Chemical Physics* 23, no. 8 (1955): 1390–1391, https://doi.org/10.1063/1.1742314.

21. G. Viswanath and M. Kasha, "Confirmation of the Anomalous Fluorescence of Azulene," *Journal of Chemical Physics* 23, no. 3 (1956): 574–577, https://doi.org/10.1063/1.1742548.

22. D. Dunlop, L. Ludvíková, A. Banerjee, H. Ottosson, and T. Slanina, "Excited-State (Anti)Aromaticity Explains Why Azulene Disobeys Kasha's Rule," *Journal of the American Chemical Society* 145 (2023): 21569–21575, https://doi.org/10.1021/jacs.3c07625.

23. F. Schwarz, M. Koch, G. Kastlunger, et al., "Ladungstransport Und Leitfähigkeitsschalten von Redoxaktiven Azulen-Derivaten," *Angewandte Chemie* 128, no. 39 (2016): 11956–11961, https://doi.org/10.1002/ange.201605559.

24. W. Thatcher Borden, H. Iwamura, and J. A. Berson, "Violations of Hund's Rule in Non-Kekuli Hydrocarbons: Theoretical Prediction and Experimental Verification," *Accounts of Chemical Research* 27 (1994): 109–116.

25. W. T. Borden and E. R. Davidson, "Theoretical Studies of Diradicals Containing Four pi Electrons," *Accounts of Chemical Research* 14 (1981): 69–76.

26. A. Borges and G. C. Solomon, "Effects of Aromaticity and Connectivity on the Conductance of Five-Membered Rings," *Journal of Physical Chemistry C* 121, no. 15 (2017): 8272–8279, https://doi.org/10.1021/acs.jpcc.7b00283.

27. P. E. M. Siegbahn, "Is There Computational Support for an Unprotonated Carbon in the E_4 State of Nitrogenase?," *Journal of Computational Chemistry* 39, no. 12 (2018): 743–747, https://doi.org/10.1002/jcc.25145.

28. D. Cho, K. C. Ko, Y. Ikabata, et al., "Effect of Hartree-Fock Exact Exchange on Intramolecular Magnetic Coupling Constants of Organic Diradicals," *Journal of Chemical Physics* 142 (2015): 024318, https://doi.org/10.1063/1.4905561.

29. K. Yamaguchi, Y. Takahara, T. Fueno, and K. Nasu, "Ab Initio MO Calculations of Effective Exchange Integrals between Transition-Metal Ions via Oxygen Dianions: Nature of the Copper-Oxygen Bonds and Superconductivity," *Japanese Journal of Applied Physics* 26, no. Part 2 (1987): L1362–L1364, https://doi.org/10.1143/JJAP.26.L1362.

30. F. Neese, "The ORCA Program System," *WIREs Computational Molecular Science* 2, no. 1 (2012): 73–78, https://doi.org/10.1002/wcms.81.

31. M. D. Hanwell, D. E. Curtis, D. C. Lonie, T. Vandermeersch, E. Zurek, and G. R. Hutchison, "Avogadro: An Advanced Semantic Chemical Editor, Visualization, and Analysis Platform," *Journal of Cheminformatics* 4, no. 1 (2012): 17, https://doi.org/10.1186/1758-2946-4-17.

32. S. Shil and D. Bhattacharya, "The Performance and Efficiency of Twelve Range-Separated Hybrid DFT Functionals for Calculation of the Magnetic Exchange Coupling Constants of Di-Nuclear First Row Transition Metal Complexes," *Computational and Theoretical Chemistry* 1235 (2024): 114541, https://doi.org/10.1016/j.comptc.2024.114541.

33. S. Shil and C. Herrmann, "Performance of Range-Separated Hybrid Exchange–Correlation Functionals for the Calculation of Magnetic Exchange Coupling Constants of Organic Diradicals," *Journal of Computational Chemistry* 39, no. 13 (2018): 780–787.

34. J. P. Perdew, J. A. Chevary, S. H. Vosko, et al., "Atoms, Molecules, Solids, and Surfaces: Applications of the Generalized Gradient Approximation for Exchange and Correlation," *Physical Review B* 46, no. 11 (1992): 6671–6687, https://doi.org/10.1103/PhysRevB.46.6671.

35. J. P. Perdew, K. Burke, and M. Ernzerhof, "Generalized Gradient Approximation Made Simple," *Physical Review Letters* 77, no. 18 (1996): 3865–3868, https://doi.org/10.1103/PhysRevLett.77.3865.

36. A. Zupan, K. Burke, M. Ernzerhof, and J. P. Perdew, "Distributions and Averages of Electron Density Parameters: Explaining the Effects of Gradient Corrections," *Journal of Chemical Physics* 106, no. 24 (1997): 10184–10193, https://doi.org/10.1063/1.474101.

37. P. H. T. Philipsen, G. te Velde, and E. J. Baerends, "The Effect of Density-Gradient Corrections for a Molecule-Surface Potential Energy Surface. Slab Calculations on Cu(100)c(2×2)-CO," *Chemical Physics Letters* 226, no. 5–6 (1994): 583–588, https://doi.org/10.1016/0009-2614(94)00735-7.

38. B. Hammer and M. Scheffler, "Local Chemical Reactivity of a Metal Alloy Surface," *Physical Review Letters* 74, no. 17 (1995): 3487–3490, https://doi.org/10.1103/PhysRevLett.74.3487.

39. B. Hammer, K. W. Jacobsen, and J. K. Nørskov, "Role of Nonlocal Exchange Correlation in Activated Adsorption," *Physical Review Letters* 70, no. 25 (1993): 3971–3974, https://doi.org/10.1103/PhysRevLett.70.3971.

40. E. I. Proynov, E. Ruiz, A. Vela, and D. R. Salahub, "Determining and Extending the Domain of Exchange and Correlation Functionals," *International Journal of Quantum Chemistry* 56, no. S29 (1995): 61–78, https://doi.org/10.1002/qua.560560808.

41. A. D. Becke, "Density-Functional Thermochemistry. III. The Role of Exact Exchange," *Journal of Chemical Physics* 98, no. 7 (1993): 5648–5652, https://doi.org/10.1063/1.464913.

42. M. de Giovanetti, L. F. F. Bitencourt, R. Cormanich, and S. P. A. Sauer, "On the Unexpected Accuracy of the M06L Functional in the Calculation of $^{1}J_{FC}$ Spin–Spin Coupling Constants," *Journal of Chemical Theory and Computation* 17, no. 12 (2021): 7712–7723, https://doi.org/10.1021/acs.jctc.1c00287.

43. D. R. Salahub and M. C. Zerner, *Quantum Chemistry Throughout the Periodic Table* (1989), 1–16, https://doi.org/10.1021/bk-1989-0394.ch001.

44. J. P. Perdew and Y. Wang, "Accurate and Simple Analytic Representation of the Electron-Gas Correlation Energy," *Physical Review B* 45, no. 23 (1992): 13244–13249, https://doi.org/10.1103/PhysRevB.45.13244.

45. J. Tao, "Exchange Energy Density of an Atom as a Functional of the Electron Density," *Journal of Chemical Physics* 115, no. 8 (2001): 3519–3530, https://doi.org/10.1063/1.1388047.

46. A. D. Becke, "A New Inhomogeneity Parameter in Density-Functional Theory," *Journal of Chemical Physics* 109, no. 6 (1998): 2092–2098, https://doi.org/10.1063/1.476722.

47. T. M. Henderson, A. F. Izmaylov, G. E. Scuseria, and A. Savin, "Assessment of a Middle-Range Hybrid Functional," *Journal of Chemical Theory and Computation* 4, no. 8 (2008): 1254–1262, https://doi.org/10.1021/ct800149y.

48. R. Peverati and D. G. Truhlar, "Improving the Accuracy of Hybrid Meta-GGA Density Functionals by Range Separation," *Journal of Physical Chemistry Letters* 2, no. 21 (2011): 2810–2817, https://doi.org/10.1021/jz201170d.

49. R. Peverati and D. G. Truhlar, "Screened-Exchange Density Functionals with Broad Accuracy for Chemistry and Solid-State Physics," *Physical Chemistry Chemical Physics* 14, no. 47 (2012): 16187, https://doi.org/10.1039/c2cp42576a.

50. J.-D. Chai and M. Head-Gordon, "Long-Range Corrected Hybrid Density Functionals with Damped Atom–Atom Dispersion Corrections," *Physical Chemistry Chemical Physics* 10, no. 44 (2008): 6615, https://doi.org/10.1039/b810189b.

51. J.-D. Chai and M. Head-Gordon, "Systematic Optimization of Long-Range Corrected Hybrid Density Functionals," *Journal of Chemical Physics* 128, no. 8 (2008): 084106, https://doi.org/10.1063/1.2834918.

52. T. M. Henderson, A. F. Izmaylov, G. Scalmani, and G. E. Scuseria, "Can Short-Range Hybrids Describe Long-Range-Dependent Properties?," *Journal of Chemical Physics* 131, no. 4 (2009): 044108, https://doi.org/10.1063/1.3185673.

53. A. V. Krukau, O. A. Vydrov, A. F. Izmaylov, and G. E. Scuseria, "Influence of the Exchange Screening Parameter on the Performance of Screened Hybrid Functionals," *Journal of Chemical Physics* 125, no. 22 (2006): 224106, https://doi.org/10.1063/1.2404663.

54. A. F. Izmaylov, G. E. Scuseria, and M. J. Frisch, "Efficient Evaluation of Short-Range Hartree-Fock Exchange in Large Molecules and Periodic Systems," *Journal of Chemical Physics* 125, no. 10 (2006): 104103, https://doi.org/10.1063/1.2347713.

55. J. Heyd, G. E. Scuseria, and M. Ernzerhof, "Hybrid Functionals Based on a Screened Coulomb Potential," *Journal of Chemical Physics* 118, no. 18 (2003): 8207–8215, https://doi.org/10.1063/1.1564060.

56. J. Heyd, J. E. Peralta, G. E. Scuseria, and R. L. Martin, "Energy Band Gaps and Lattice Parameters Evaluated with the Heyd-Scuseria-Ernzerhof Screened Hybrid Functional," *Journal of Chemical Physics* 123, no. 17 (2005): 174101, https://doi.org/10.1063/1.2085170.

57. J. Heyd and G. E. Scuseria, "Assessment and Validation of a Screened Coulomb Hybrid Density Functional," *Journal of Chemical Physics* 120, no. 16 (2004): 7274–7280, https://doi.org/10.1063/1.1668634.

58. J. Heyd and G. E. Scuseria, "Efficient Hybrid Density Functional Calculations in Solids: Assessment of the Heyd–Scuseria–Ernzerhof Screened Coulomb Hybrid Functional," *Journal of Chemical Physics* 121, no. 3 (2004): 1187–1192, https://doi.org/10.1063/1.1760074.

59. O. A. Vydrov, G. E. Scuseria, and J. P. Perdew, "Tests of Functionals for Systems with Fractional Electron Number," *Journal of Chemical Physics* 126, no. 15 (2007): 154109, https://doi.org/10.1063/1.2723119.

60. O. A. Vydrov and G. E. Scuseria, "Assessment of a Long-Range Corrected Hybrid Functional," *Journal of Chemical Physics* 125, no. 23 (2006): 234109, https://doi.org/10.1063/1.2409292.

61. O. A. Vydrov, J. Heyd, A. V. Krukau, and G. E. Scuseria, "Importance of Short-Range versus Long-Range Hartree-Fock Exchange for the Performance of Hybrid Density Functionals," *Journal of Chemical Physics* 125, no. 7 (2006): 074106, https://doi.org/10.1063/1.2244560.

62. T. Yanai, D. P. Tew, and N. C. Handy, "A New Hybrid Exchange–Correlation Functional Using the Coulomb-Attenuating Method (CAM-B3LYP)," *Chemical Physics Letters* 393, no. 1–3 (2004): 51–57, https://doi.org/10.1016/j.cplett.2004.06.011.

63. S. Grimme, "Semiempirical Hybrid Density Functional with Perturbative Second-Order Correlation," *Journal of Chemical Physics* 124, no. 3 (2006): 034108, https://doi.org/10.1063/1.2148954.

64. M. Casanova-Páez, M. B. Dardis, and L. Goerigk, "Ωb2PLYP and Ωb2GPPLYP: The First Two Double-Hybrid Density Functionals with Long-Range Correction Optimized for Excitation Energies," *Journal of Chemical Theory and Computation* 15, no. 9 (2019): 4735–4744, https://doi.org/10.1021/acs.jctc.9b00013.

65. C. Lee, e. Yang, and R. G. Parr, "Development of the Colic-Salvetti Correlation-Energy Formula into a Functional of the Electron Density," *Physical Review B* 37 (1988): 785.

66. S. Shil and C. Herrmann, "Increasing Magnetic Coupling through Oxidation of a Ferrocene Bridge," *Inorganic Chemistry* 54, no. 24 (2015): 11733–11740, https://doi.org/10.1021/acs.inorgchem.5b01707.

67. J. R. Dias, "Disjoint Molecular Orbitals in Nonalternant Conjugated Diradical Hydrocarbons," *Journal of Chemical Information and Computer Sciences* 43, no. 5 (2003): 1494–1501, https://doi.org/10.1021/ci034056z.

68. W. T. Borden and E. R. Davidson, "Effects of Electron Repulsion in Conjugated Hydrocarbon Diradicals," *Journal of the American Chemical Society* 99, no. 14 (1977): 4587–4594, https://doi.org/10.1021/ja00456a010.

69. W. T. Borden and E. R. Davidson, "Theoretical Studies of Diradicals Containing Four .Pi. Electrons," *Accounts of Chemical Research* 14, no. 3 (1981): 69–76, https://doi.org/10.1021/ar00063a002.

Supporting Information

Additional supporting information can be found online in the Supporting Information section.